Available online at www.sciencedirect.com
SCIENCE DIRECT
Journal of Computational Physics 215 (2006) 81–97
JOURNAL OF COMPUTATIONAL PHYSICS
www.elsevier.com/locate/jcp

Stable coupling between vector and scalar variables for the IDO scheme on collocated grids

Yohsuke Imai *, Takayuki Aoki

Global Scientific Information and Computing Center, Tokyo Institute of Technology, 2-12-1 O-okayama, Meguro-ku, Tokyo 152-8550, Japan

Received 24 May 2005; received in revised form 30 September 2005; accepted 21 October 2005
Available online 6 December 2005

Abstract

The Interpolated Differential Operator (IDO) scheme on collocated grids provides fourth-order discretizations for all the terms of the fluid flow equations. However, computations of fluid flows on collocated grids are not guaranteed to produce accurate solutions because of the poor coupling between velocity vector and scalar variables. A stable coupling method for the IDO scheme on collocated grids is proposed, where a new representation of first-order derivatives is adopted. It is important in deriving the representation to refer to the variables at neighboring grid points, keeping fourth-order truncation error. It is clear that accuracy and stability are drastically improved for shallow water equations in comparison with the conventional IDO scheme. The effects of the stable coupling are confirmed in incompressible flow calculations for DNS of turbulence and a driven cavity problem. The introduction of a rational function into the proposed method makes it possible to calculate shock waves with the initial conditions of extreme density and pressure jumps.

PACS: 02.60.−x; 02.60.Cb; 02.70.Rw

Keywords: IDO scheme; Numerical coupling; Collocated grid; Computational fluid dynamics; Numerical stability; Higher-order accuracy

1. Introduction

Many physical processes are modeled by partial differential equations (PDEs) with more than one dependent variable. The Navier–Stokes equation, which describes fluid motion, consists of velocity vector and scalar variables of pressure and density. Numerical coupling between the vector and scalar variables is the key issue to successfully obtain highly accurate solutions. In finite element computations of fluid flows, the coupling is handled by using the pressure-stabilizing/Petrov–Galerkin (PSPG) formulation [1,2]. For finite difference schemes, staggered grids provide good coupling and have been adopted in many numerical methods such as the Marker-and-Cell (MAC) method [3] and the Semi-Implicit Method for Pressure-Linked Equations (SIMPLE) [4].

* Corresponding author. Tel.: +81 3 5734 3575; fax: +81 3 5734 3276.
E-mail address: yimai@sim.gsic.titech.ac.jp (Y. Imai).

0021-9991/$ - see front matter © 2005 Elsevier Inc. All rights reserved.
doi:10.1016/j.jcp.2005.10.015

We have developed the Interpolated Differential Operator (IDO) scheme [5–8], which solves not only physical variables but also first-order spatial derivatives as additional dependent variables. The scheme uses the Hermite interpolation function that is thought to be an approximated solution of the given PDE. The major difference from the Compact Difference (CD) scheme [9] is the calculation for first-order derivatives. While in the CD scheme derivatives at each grid point are implicitly given by the relation matrix to neighboring grid points, first-order derivatives of the IDO scheme are given as the solutions of additional equations which are derived from governing equations. The first-order derivatives of the IDO scheme make the resolved wavenumber wider than the Finite Difference (FD) and CD schemes. Staggered grids have been used in the fluid flow analysis of the IDO scheme for numerical coupling, but staggered grids reduce spatial accuracy to second-order. In contrast, the IDO scheme on collocated grids retains fourth-order accuracy in space. Collocated grids offer conspicuous advantages for formulation, programming, parallel computing, treatment of boundary conditions and unstructured grids, and for the application to advanced methods such as the Adaptive Mesh Refinement (AMR) method [10,11] and the Cut-Cell method [12,13]. However, calculations on collocated grids can sometimes become unstable, because the first-order derivatives in the governing equations are given as dependent variables and therefore do not refer to neighboring grid points directly. In particular, collocated grids could not be applied to shock problems with initial jump conditions.

In this paper, we propose a stable coupling method for the IDO scheme on collocated grids (IDO-SC scheme), where a new representation of the first-order derivative is adopted. The IDO-SC scheme improves accuracy and stability for the shallow water equations in a hydrostatic meteorological model and for incompressible flow simulations. A rational function is introduced into the IDO-SC scheme to calculate extremely strong shock waves.

2. Formulation of the IDO-SC scheme

2.1. Review of the IDO scheme

We consider the following two equations couple to each other:

$$\frac{\partial f}{\partial t} = \frac{\partial u}{\partial x}, \tag{2.1}$$

$$\frac{\partial u}{\partial t} = \frac{\partial f}{\partial x}, \tag{2.2}$$

which are equivalent to one-dimensional wave equations with unit phase speed. The additional equations derived by taking the differentiation of the above equations are solved for the time evolution of the first-order spatial derivatives:

$$\frac{\partial f_x}{\partial t} = \frac{\partial^2 u}{\partial x^2}, \tag{2.3}$$

$$\frac{\partial u_x}{\partial t} = \frac{\partial^2 f}{\partial x^2}. \tag{2.4}$$

The subscript x in Eqs. (2.3) and (2.4) represents the spatial derivative in the x-direction where $f_x \equiv \partial f/\partial x$ and $u_x \equiv \partial u/\partial x$. To solve Eqs. (2.1)–(2.4), we need to discretize the first- and second-order derivatives. We briefly review the discretizations of the conventional IDO scheme on staggered grids and collocated grids.

The physical variable f and the first-order derivative f_x are defined at a grid point j as f_j and $f_{x,j}$ in the computational domain of $x_0 < x < x_N$ with an uniform grid spacing $h = x_{j+1} - x_j$. On staggered grids, the physical variable u and the first-order derivative u_x are defined at a cell-centered point as $u_{j+1/2}$ and $u_{x,j+1/2}$.

A cubic interpolation function is used to obtain derivatives at the cell-centered point:

$$F(X) = A_3X^3 + A_2X^2 + A_1X + A_0, \tag{2.5}$$

where $X = x - x_{j+1/2}$. The coefficients of Eq. (2.5) are determined with the constraints of $F(h/2) = f_{j+1}$, $F(-h/2) = f_j$, $F_x(h/2) = f_{x,j+1}$, and $F_x(-h/2) = f_{x,j}$ as

$$A_3 = -\frac{2}{h^3}(f_{j+1} - f_j) + \frac{1}{h^2}(f_{x,j+1} + f_{x,j}), \tag{2.6}$$

$$A_2 = \frac{1}{h}(f_{x,j+1} - f_{x,j}), \tag{2.7}$$

$$A_1 = \frac{3}{2h}(f_{j+1} - f_j) - \frac{1}{4}(f_{x,j+1} + f_{x,j}), \tag{2.8}$$

$$A_0 = \frac{1}{2}(f_{j+1} + f_j) - \frac{h}{8}(f_{x,j+1} - f_{x,j}). \tag{2.9}$$

First- and second-order derivatives at $x = x_{j+1/2}$ are derived from the interpolation function as $f_x(x_j) = F_x(0) = A_1$, and $f_{xx}(x_j) = F_{xx}(0) = 2A_2$. Eqs. (2.1)–(2.4) are discretized by

$$\left.\frac{\partial f}{\partial t}\right|_j = \frac{3}{2h}(u_{j+1/2} - u_{j-1/2}) - \frac{1}{4}(u_{x,j+1/2} + u_{x,j-1/2}), \tag{2.10}$$

$$\left.\frac{\partial u}{\partial t}\right|_{j+1/2} = \frac{3}{2h}(f_{j+1} - f_j) - \frac{1}{4}(f_{x,j+1} + f_{x,j}), \tag{2.11}$$

$$\left.\frac{\partial f_x}{\partial t}\right|_j = \frac{1}{h}(u_{x,j+1/2} - u_{x,j-1/2}), \tag{2.12}$$

$$\left.\frac{\partial u_x}{\partial t}\right|_{j+1/2} = \frac{1}{h}(f_{x,j+1} - f_{x,j}). \tag{2.13}$$

Unfortunately, Eqs. (2.12) and (2.13) reduce to second-order central finite differences and the overall accuracy of the calculation becomes only second-order.

With collocated grids, all the variables f, f_x, u, and u_x are defined at a same grid point as f_j, $f_{x,j}$, u_j, and $u_{x,j}$. We can construct a fifth-order interpolation function over the minimum domain $x_{j-1} < x < x_{j+1}$:

$$F(X) = B_5X^5 + B_4X^4 + B_3X^3 + B_2X^2 + B_1X + B_0, \tag{2.14}$$

where $X = x - x_j$. The unknown coefficients of Eq. (2.14) are calculated with the constraints $F(0) = f_j$, $F_x(0) = f_{x,j}$, $F(\pm h) = f_{j\pm1}$, and $F_x(\pm h) = f_{x,j\pm1}$:

$$B_5 = -\frac{3}{4h^5}(f_{j+1} - f_{j-1}) + \frac{1}{4h^4}(f_{x,j+1} + 4f_{x,j} + f_{x,j-1}), \tag{2.15}$$

$$B_4 = -\frac{1}{2h^4}(f_{j+1} - 2f_j + f_{j-1}) + \frac{1}{4h^3}(f_{x,j+1} - f_{x,j-1}), \tag{2.16}$$

$$B_3 = \frac{5}{4h^3}(f_{j+1} - f_{j-1}) - \frac{1}{4h^2}(f_{x,j+1} + 8f_{x,j} + f_{x,j-1}), \tag{2.17}$$

$$B_2 = \frac{1}{h^2}(f_{j+1} - 2f_j + f_{j-1}) - \frac{1}{4h}(f_{x,j+1} - f_{x,j-1}), \tag{2.18}$$

$$B_1 = f_{x,j}, \tag{2.19}$$

$$B_0 = f_j. \tag{2.20}$$

By using the first-order derivative $f_x(x_j) = F_x(0) = B_1$ and the second-order derivative $f_{xx}(x_j) = F_{xx}(0) = 2B_2$, Eqs. (2.1)–(2.4) are expressed as follows:

$$\left.\frac{\partial f}{\partial t}\right|_j = u_{x,j}, \tag{2.21}$$

$$\left.\frac{\partial u}{\partial t}\right|_j = f_{x,j}, \tag{2.22}$$

$$\left.\frac{\partial f_x}{\partial t}\right|_j = \frac{2}{h^2}(u_{j+1} - 2u_j + u_{j-1}) - \frac{1}{2h}(u_{x,j+1} - u_{x,j-1}), \tag{2.23}$$

$$\left.\frac{\partial u_x}{\partial t}\right|_j = \frac{2}{h^2}(f_{j+1} - 2f_j + f_{j-1}) - \frac{1}{2h}(f_{x,j+1} - f_{x,j-1}). \tag{2.24}$$

Poor coupling between f and u comes from Eqs. (2.21) and (2.22), where the right-hand sides of these equations do not include the variables at neighboring grid points $j+1$ and $j-1$.

2.2. New representation of the first-order derivative

The Taylor series expansion of the physical variable $f(x)$ at a position $x = x_j$ is considered:

$$f(x_j + \mathrm{d}x) = f(x_j) + \left.\frac{\partial f}{\partial x}\right|_{x=x_j} \mathrm{d}x + \left.\frac{1}{2}\frac{\partial^2 f}{\partial x^2}\right|_{x=x_j} \mathrm{d}x^2 + \left.\frac{1}{6}\frac{\partial^3 f}{\partial x^3}\right|_{x=x_j} \mathrm{d}x^3 + \cdots \tag{2.25}$$

Substituting $f(x_j) = f_j$ into the equation, we have

$$f(x_j + \mathrm{d}x) = f_j + \left.\frac{\partial f}{\partial x}\right|_{x=x_j} \mathrm{d}x + \left.\frac{1}{2}\frac{\partial^2 f}{\partial x^2}\right|_{x=x_j} \mathrm{d}x^2 + \left.\frac{1}{6}\frac{\partial^3 f}{\partial x^3}\right|_{x=x_j} \mathrm{d}x^3 + \cdots \tag{2.26}$$

For the first-order derivative $f_x(x)$, the Taylor series at the position $x = x_j$ is expressed as

$$f_x(x_j + \mathrm{d}x) = f_x(x_j) + \left.\frac{\partial^2 f}{\partial x^2}\right|_{x=x_j} \mathrm{d}x + \left.\frac{1}{2}\frac{\partial^3 f}{\partial x^3}\right|_{x=x_j} \mathrm{d}x^2 + \left.\frac{1}{6}\frac{\partial^4 f}{\partial x^4}\right|_{x=x_j} \mathrm{d}x^3 + \cdots \tag{2.27}$$

Using $f_x(x_j) = f_{x,j}$, the expression is rewritten by

$$f_x(x_j + \mathrm{d}x) = f_{x,j} + \left.\frac{\partial^2 f}{\partial x^2}\right|_{x=x_j} \mathrm{d}x + \left.\frac{1}{2}\frac{\partial^3 f}{\partial x^3}\right|_{x=x_j} \mathrm{d}x^2 + \left.\frac{1}{6}\frac{\partial^4 f}{\partial x^4}\right|_{x=x_j} \mathrm{d}x^3 + \cdots \tag{2.28}$$

The discretized formula of the first-order derivative at the position $x = x_j$ is obtained from Eqs. (2.26) and (2.28) with the constraints of $f(x_j - h_m) = f_{j-1}$, $f(x_j + h_p) = f_{j+1}$, $f_x(x_j - h_m) = f_{x,j-1}$ and $f_x(x_j + h_p) = f_{x,j+1}$, where $h_p = x_{j+1} - x_j$ and $h_m = x_j - x_{j-1}$. In the case of uniform grid spacing $h_p = h_m = h$, Eq. (2.26) leads to the second-order finite difference,

$$\left.\frac{\partial f}{\partial x}\right|_{x=x_j} = \frac{1}{2h}(f_{j+1} - f_{j-1}) - \left.\frac{1}{6}\frac{\partial^3 f}{\partial x^3}\right|_{x=x_j} h^2 - \left.\frac{1}{120}\frac{\partial^5 f}{\partial x^5}\right|_{x=x_j} h^4 + \cdots \tag{2.29}$$

The third-order derivative approximation is given by Eq. (2.28):

$$\left.\frac{\partial^3 f}{\partial x^3}\right|_{x=x_j} = \frac{1}{h^2}(f_{x,j+1} - 2f_{x,j} + f_{x,j-1}) - \left.\frac{1}{12}\frac{\partial^5 f}{\partial x^5}\right|_{x=x_j} h^2 + \cdots \tag{2.30}$$

Substituting Eq. (2.30) into Eq. (2.29), the following discretized formula of the first-order derivative is obtained:

$$\left.\frac{\partial f}{\partial x}\right|_{x=x_j} = \frac{1}{2h}(f_{j+1} - f_{j-1}) - \frac{1}{6}(f_{x,j+1} - 2f_{x,j} + f_{x,j-1}) + \left.\frac{1}{180}\frac{\partial^5 f}{\partial x^5}\right|_{x=x_j} h^4 + \cdots \tag{2.31}$$

This representation of the first-order derivative refers to both the physical variables and the first-order derivatives at neighboring grid points, and has fourth-order truncation error. In the IDO-SC scheme, coupling terms such as pressure gradient and divergence of velocity are discretized by using Eq. (2.31).

2.3. Relation to the interpolation function

Without the constraint $F_x(x_j) = f_{x,j}$, a fourth-order polynomial,

$$F(x) = C_4X^4 + C_3X^3 + C_2X^2 + C_1X + C_0, \tag{2.32}$$

can be constructed. The coefficients of Eq. (2.32) are determined by the five constraints $F(0) = f_j$, $F(\pm h) = f_{j\pm1}$, and $F_x(\pm h) = f_{x,j\pm1}$:

$$C_4 = -\frac{1}{2h^4}(f_{j+1} - 2f_j + f_{j-1}) + \frac{1}{4h^3}(f_{x,j+1} - f_{x,j-1}), \tag{2.33}$$

$$C_3 = -\frac{1}{4h^3}(f_{j+1} - f_{j-1}) + \frac{1}{4h^2}(f_{x,j+1} + f_{x,j-1}), \tag{2.34}$$

$$C_2 = \frac{1}{h^2}(f_{j+1} - 2f_j + f_{j-1}) - \frac{1}{4h}(f_{x,j+1} - f_{x,j-1}), \tag{2.35}$$

$$C_1 = \frac{3}{4h}(f_{j+1} - f_{j-1}) - \frac{1}{4}(f_{x,j+1} + f_{x,j-1}), \tag{2.36}$$

$$C_0 = f_j. \tag{2.37}$$

First- and second-order derivatives at $x = x_j$ are given as $f_x(x_j) = F_x(0) = C_1$ and $f_{xx}(x_j) = F_{xx}(0) = 2C_2$, respectively. Using the weighted average of these derivatives and the corresponding derivatives of the fifth-order interpolation function (2.14), we have

$$f_x(x_j) = (1 - \alpha)B_1 + \alpha C_1, \tag{2.38}$$

and

$$f_{xx}(x_j) = 2\{(1 - \beta)B_2 + \beta C_2\}. \tag{2.39}$$

Because $B_2 = C_2$, the weighted average with β is meaningless for the second-order derivative. When we use the weighted factor $\alpha = 2/3$, this first-order derivative is coincident with the SC representation (2.31). We can interpret the above as follows: the spatial profiles of the dependent variables are expressed by the combination of the fifth-order interpolation function (2.14) and the fourth-order interpolation function (2.32).

2.4. The IDO-SC scheme in multi-dimensional case

For two-dimensional wave equations written by

$$\frac{\partial f}{\partial t} = \frac{\partial u}{\partial x} + \frac{\partial v}{\partial y}, \tag{2.40}$$

$$\frac{\partial u}{\partial t} = \frac{\partial f}{\partial x}, \tag{2.41}$$

$$\frac{\partial v}{\partial t} = \frac{\partial f}{\partial y}, \tag{2.42}$$

we solve f_x, f_y, f_{xy}, u_x, u_y, u_{xy}, v_x, v_y, and v_{xy} as dependent variables using the following equations:

$$\frac{\partial f_x}{\partial t} = \frac{\partial^2 u}{\partial x^2} + \frac{\partial^2 v}{\partial x \partial y}, \tag{2.43}$$

$$\frac{\partial f_y}{\partial t} = \frac{\partial^2 u}{\partial x \partial y} + \frac{\partial^2 v}{\partial y^2}, \tag{2.44}$$

$$\frac{\partial f_{xy}}{\partial t} = \frac{\partial^3 u}{\partial x^2 \partial y} + \frac{\partial^3 v}{\partial x \partial y^2}, \tag{2.45}$$

$$\frac{\partial u_x}{\partial t} = \frac{\partial^2 f}{\partial x^2}, \tag{2.46}$$

$$\frac{\partial u_y}{\partial t} = \frac{\partial^2 f}{\partial x \partial y}, \tag{2.47}$$

$$\frac{\partial u_{xy}}{\partial t} = \frac{\partial^3 f}{\partial x^2 \partial y}, \tag{2.48}$$

$$\frac{\partial v_x}{\partial t} = \frac{\partial^2 f}{\partial x \partial y}, \tag{2.49}$$

$$\frac{\partial v_y}{\partial t} = \frac{\partial^2 f}{\partial y^2}, \tag{2.50}$$

$$\frac{\partial v_{xy}}{\partial t} = \frac{\partial^3 f}{\partial x \partial y^2}. \tag{2.51}$$

The representation of the first-order derivative (2.31) is applied to the derivative terms on the right-hand sides of Eqs. (2.40)–(2.42). The second-order cross derivatives of v_{xy} and f_{xy} in Eqs. (2.43) and (2.49) are considered to be the first-order derivative of v_y and f_y in the x-direction. For uniform grid spacing $x_{j+1} - x_j = h$, the following form is substituted into to the cross derivative terms:

$$\left.\frac{\partial^2 f}{\partial x \partial y}\right|_{x=x_i, y=y_j} = \frac{1}{2h}(f_{y,i+1,j} - f_{y,i-1,j}) - \frac{1}{6}(f_{xy,i+1,j} - 2f_{xy,i,j} + f_{xy,i-1,j}). \tag{2.52}$$

The cross derivative terms in Eqs. (2.44) and (2.47) are considered to be the first-order derivative of u_x and f_x in the y-direction, and are discretized by

$$\left.\frac{\partial^2 f}{\partial x \partial y}\right|_{x=x_i, y=y_j} = \frac{1}{2h}(f_{x,i,j+1} - f_{x,i,j-1}) - \frac{1}{6}(f_{xy,i,j+1} - 2f_{xy,i,j} + f_{xy,i,j-1}), \tag{2.53}$$

in the case of uniform grid spacing $y_{j+1} - y_j = h$. The other derivatives on the right-hand sides of the equations are discretized by the fifth-order interpolation function used in the conventional IDO scheme.

3. Numerical accuracy of the IDO-SC scheme

3.1. Fourier analysis

Fourier analysis is carried out for the first-order derivative (2.31). The spatial profile of the dependent variable $f(x)$ is assumed to be periodic over the domain $[0, L]$ with uniform grid spacing $h = L/N$. The dependent variable may be decomposed into a Fourier series,

$$f(x) = \sum_k \hat{f}(k) \mathrm{e}^{\mathrm{i}wx/h}, \tag{3.1}$$

where $\mathrm{i} = \sqrt{-1}$, and $w = 2\pi kh/L$ is a scaled wavenumber. In the IDO-SC scheme, the first-order derivative is solved independently, and the spatial profile of the first-order derivative is described as

$$f_x(x) = \sum_k \hat{f}_x(k) \mathrm{e}^{\mathrm{i}wx/h}. \tag{3.2}$$

The physical variables and the first-order derivatives at grid points j and $j \pm 1$ are given by

$$f_j = f(x_j) = \sum_k \hat{f}(k) \mathrm{e}^{\mathrm{i}wx_j/h}, \tag{3.3}$$

$$f_{x,j} = f_x(x_j) = \sum_k \hat{f}_x(k) \mathrm{e}^{\mathrm{i}wx_j/h}, \tag{3.4}$$

$$f_{j\pm1} = f(x_j \pm h) = \sum_k \hat{f}(k) \mathrm{e}^{\mathrm{i}wx_j/h} \mathrm{e}^{\pm \mathrm{i}w}, \tag{3.5}$$

$$f_{x,j\pm1} = f_x(x_j \pm h) = \sum_k \hat{f}_x(k) \mathrm{e}^{\mathrm{i}wx_j/h} \mathrm{e}^{\pm \mathrm{i}w}. \tag{3.6}$$

Substituting Eqs. (3.3)–(3.6) into Eq. (2.31), we have

$$f_x^{\mathrm{SC}}(x_j) = \sum_k \frac{\mathrm{i}\sin w}{h} \hat{f}(k) \mathrm{e}^{\mathrm{i}wx_j/h} - \sum_k \frac{\cos w - 1}{3} \hat{f}_x(k) \mathrm{e}^{\mathrm{i}wx_j/h}. \tag{3.7}$$

Here, we assume the Fourier coefficient $\hat{f}_x(k)$ to be $\hat{f}_x(k) = \mathrm{i}(w/h)\hat{f}(k)$. Eq. (3.7) reduces to

$$f_x^{\mathrm{SC}}(x_j) = \sum_k \mathrm{i}\left(\frac{3\sin w + w - w\cos w}{3h}\right)\hat{f}(k)\mathrm{e}^{\mathrm{i}wx_j/h}. \tag{3.8}$$

Lele [9] introduced the modified wavenumber w_m. The first-order derivative is described with the modified wavenumber as

$$f_x^{\mathrm{SC}}(x_j) = \sum_k \hat{f}_x^{\mathrm{SC}}(k)\mathrm{e}^{\mathrm{i}wx_j/h} = \sum_k \mathrm{i}\left(\frac{w_m}{h}\right)\hat{f}(k)\mathrm{e}^{\mathrm{i}wx_j/h}, \tag{3.9}$$

where the modified wavenumber for Eq. (3.8) is estimated by

$$w_m = \sin w + \frac{w}{3} - \frac{w\cos w}{3}. \tag{3.10}$$

Plots of the modified wavenumber against the exact wavenumber are presented in Fig. 1 in comparison with second-, fourth-, and sixth-order FD schemes, and a fourth-order CD scheme [9]. It is found that the modified wavenumber for the IDO-SC scheme is the closest to the exact wavenumber among the other difference schemes for a wide range of wavenumber.

3.2. Wave equation

We examine the numerical accuracy of the IDO-SC scheme for one-dimensional wave equations with positive constant $c = 1.0$ as the simplest coupling problem:

$$\frac{\partial^2 f}{\partial t^2} = c^2\frac{\partial^2 f}{\partial x^2}. \tag{3.11}$$

This equation is divided into Eqs. (2.1) and (2.2). For the periodic domain [0, 1] with uniform grid spacing $h = 1/N$, the initial condition is set to be

$$f(0,x) = A\sin\left(-\frac{w}{h}x\right) + B\cos\left(\frac{w}{h}x\right), \tag{3.12}$$

$$u(0,x) = -A\sin\left(-\frac{w}{h}x\right) + B\cos\left(\frac{w}{h}x\right), \tag{3.13}$$

where the coefficients $A = 0.8$, $B = 0.2$ are chosen. We estimate the averaged error at the time $t = 1/k$ using the following equation:

$$\text{error} = \sum_N |f_{\text{exact},j} - f_{\text{numerical},j}|h, \tag{3.14}$$

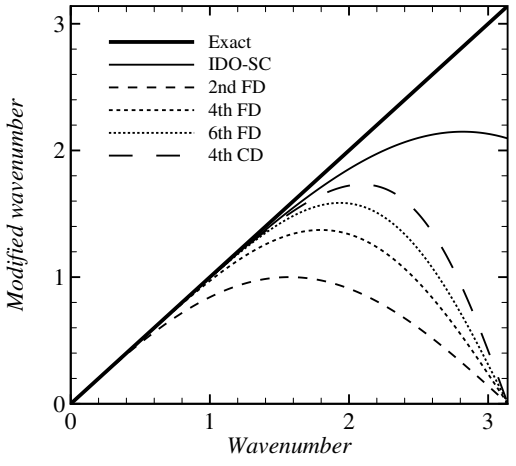

Fig. 1. Modified wavenumber for first-order derivative approximations.

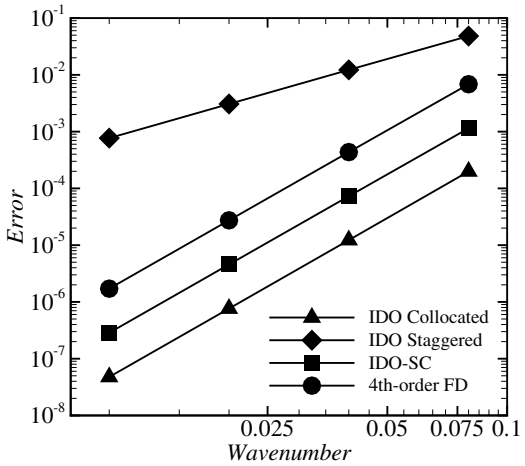

Fig. 2. Numerical errors of one-dimensional wave equations.

where $f_{\text{exact},j}$ and $f_{\text{numerical},j}$ denote the exact solution and the numerical solution, respectively. In Fig. 2, the deviation errors of the N1 norm from the exact solution is shown for the IDO-SC scheme, the conventional IDO scheme on staggered grids and collocated grids, and the fourth-order FD scheme. The error for the staggered grid IDO scheme indicates a second-order slope against the wavenumber. The other schemes have fourth-order accuracy. The amplitude of the error of the IDO-SC scheme is one-order of magnitude smaller than that of the FD scheme, and one-order larger than that of the conventional IDO scheme on collocated grids.

4. Shallow water problem

Shallow water equations are often solved for weather forecast in hydrostatic meteorological models or ocean problems. It is important to calculate the gravity wave with high accuracy and stability. We introduce the proposed method for coupling between the geopotential height field and wind velocity components. Shallow water equations over a rotating sphere, using Cartesian coordinates on a polar stereographic projection, are described as

$$\frac{\partial U}{\partial t} = -SU\frac{\partial U}{\partial x} - SV\frac{\partial U}{\partial y} - \frac{\partial \phi}{\partial x} + fV - \frac{1}{2}\frac{\partial S}{\partial x}(U^2 + V^2), \tag{4.1}$$

$$\frac{\partial V}{\partial t} = -SU\frac{\partial V}{\partial x} - SV\frac{\partial V}{\partial y} - \frac{\partial \phi}{\partial y} - fU - \frac{1}{2}\frac{\partial S}{\partial y}(U^2 + V^2), \tag{4.2}$$

$$\frac{\partial \phi}{\partial t} = -SU\frac{\partial \phi}{\partial x} - SV\frac{\partial \phi}{\partial y} + \phi S\left(\frac{\partial U}{\partial x} + \frac{\partial V}{\partial y}\right), \tag{4.3}$$

where $U = u/m$, and $V = v/m$ are termed the wind images, u and v are the components of the wind vector in the x-direction and the y-direction, respectively. The notation m is the map-scale factor, and $S = m^2$, ϕ is the geopotential height of the free surface, and $f = 2\Omega\sin(\text{lat})$ is the Coriolis parameter with the latitude coordinates 'lat'. For these equations, the SC discretization (2.31) is used for $\partial\phi/\partial x$ in Eq. (4.1), $\partial\phi/\partial y$ in Eq. (4.2), and $\partial U/\partial x$ and $\partial V/\partial y$ in Eq. (4.3). We also time advance the derivatives U_x, U_y, U_{xy}, V_x, V_y, V_{xy}, ϕ_x, ϕ_y, and ϕ_{xy} by solving the differentiated equations corresponding to Eqs. (4.1)–(4.3). We apply the third-order upwind interpolation function used in the Constrained Interpolation Profile (CIP) scheme [14–17] to the second-order derivatives derived from the advection terms.

The model is run over a square domain 200,000 km on each side centered at the North Pole, using a stereographic projection true at 60°N. We use the same initial condition as reference [18,19], which is based on an operational 500 mb analysis for 12:00 GMT on 28 February 1984. Uniform collocated grids are used, and the solid wall boundary conditions are given in the vicinity of the equator. In order to show boundary

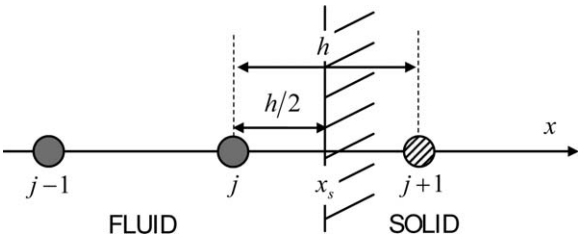

Fig. 3. Schematic for wall boundary treatment.

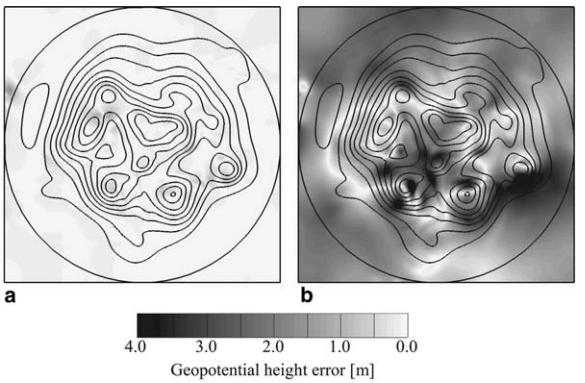

Fig. 4. Maps of root mean square differences from the result of Temperton for the geopotential height shown by contours: (a) the IDO-SC scheme; (b) the conventional IDO scheme. A circle outside the contours represents the equator.

treatments, the vertical wall illustrated in Fig. 3 is considered, where the wall surface is located at a cell-centered point $x = x_s$. Imaginary fluid variables at the grid point $j+1$ are extrapolated as follows:

$$U_{j+1} = -U_j, \quad U_{x,j+1} = U_{x,j}, \quad U_{y,j+1} = -U_{y,j}, \quad U_{xy,j+1} = U_{xy,j}, \tag{4.4}$$

$$V_{j+1} = -V_j, \quad V_{x,j+1} = V_{x,j}, \quad V_{y,j+1} = -V_{y,j}, \quad V_{xy,j+1} = V_{xy,j}, \tag{4.5}$$

$$\phi_{j+1} = \phi_j, \quad \phi_{x,j+1} = -\phi_{x,j}, \quad \phi_{y,j+1} = \phi_{y,j}, \quad \phi_{xy,j+1} = -\phi_{xy,j}. \tag{4.6}$$

In the case of the horizontal wall, the same procedure is adopted.

We compare the geopotential height errors of the IDO-SC scheme with those of the conventional IDO scheme after 2 days. The errors are measured by the root mean square differences from the high-resolution results of Temperton [19] using 25 km resolution grids. Fig. 4(a) and (b) show the error maps of the IDO-SC scheme and the IDO scheme with 200 km resolution grids. The errors are greatly reduced by using the IDO-SC scheme. In spite of using eight times coarser grids, the same accurate results are obtained as in the method by Temperton.

5. Incompressible flow problem

5.1. DNS of two-dimensional homogeneous isotropic turbulence

Direct Numerical Simulation (DNS) of homogeneous isotropic turbulence is a suitable problem for checking the numerical accuracy of incompressible flow simulations. The results are compared with that of a spectral method [20]. The governing equations are described as

$$\frac{\partial \mathbf{u}}{\partial t} = -(\mathbf{u}\cdot\nabla)\mathbf{u} - \nabla p + \frac{1}{Re}\nabla^2\mathbf{u}, \tag{5.1}$$

$$\nabla\cdot\mathbf{u} = 0. \tag{5.2}$$

The time integration is done by a four-stage explicit Runge–Kutta method:

$$\mathbf{u}^{n+1} = \mathbf{u}^n + \sum_p^4 \beta_p \mathbf{k}_p \Delta t, \tag{5.3}$$

where $(\beta_1 \quad \beta_2 \quad \beta_3 \quad \beta_4) = (1/6 \quad 1/3 \quad 1/3 \quad 1/6)$. The time derivative $\mathbf{k}_p$ is calculated by the Simplified-MAC (SMAC) [21] type method:

$$\mathbf{k}_p = \mathbf{k}_p^* - \nabla p^p, \tag{5.4}$$

$$\mathbf{k}_p^* = -(\mathbf{u}^p \cdot \nabla)\mathbf{u}^p + \frac{1}{Re}\nabla^2 \mathbf{u}^p, \tag{5.5}$$

where

$$\mathbf{u}^p = \mathbf{u}^n + \sum_q^4 \alpha_{pq} \mathbf{k}_q \Delta t, \tag{5.6}$$

and

$$\begin{pmatrix} \alpha_{11} & \alpha_{12} & \alpha_{13} & \alpha_{14} \\ \alpha_{21} & \alpha_{22} & \alpha_{23} & \alpha_{24} \\ \alpha_{31} & \alpha_{32} & \alpha_{33} & \alpha_{34} \\ \alpha_{41} & \alpha_{42} & \alpha_{43} & \alpha_{44} \end{pmatrix} = \begin{pmatrix} 0 & 0 & 0 & 0 \\ 1/2 & 0 & 0 & 0 \\ 0 & 1/2 & 0 & 0 \\ 0 & 0 & 1 & 0 \end{pmatrix}.$$

Eq. (5.3) must satisfy the divergence free condition (5.2), and the following Poisson equation is therefore solved by a multigrid SOR method [8]:

$$\nabla \cdot \mathbf{k}_p^* = \nabla^2 p^p. \tag{5.7}$$

For the time integration of derivatives $\mathbf{u}_x$, $\mathbf{u}_y$, and $\mathbf{u}_{xy}$, we calculate $\mathbf{k}_{x,p}$, $\mathbf{k}_{y,p}$, and $\mathbf{k}_{xy,p}$ with the differentiated equations of Eqs. (5.4), (5.5) and (5.7). In these equations, stable coupling is applied to the coupling terms, that is, the pressure gradient of Eq. (5.4), the divergence of the velocity in Eq. (5.7), and the corresponding second-order cross derivatives of these coupling terms as shown in Section 2.4. The other terms such as advection and diffusion terms and the right-hand side of Poisson Eq. (5.7) are discretized by using the fifth-order central interpolation function (2.14).

We use 512×512 collocated grids for the computational domain of $0 \leqslant x \leqslant 1$ and $0 \leqslant y \leqslant 1$. The same initial condition and the time interval $\Delta t = 8.2928 \times 10^{-5}$ are employed as the spectral method. The initial energy spectrum is shown in Fig. 5. The Reynolds number is 10930.8 ($Re_{\lambda_0} = 396.251$), where the notation λ_0 represents the Taylor micro-scale in the initial condition.

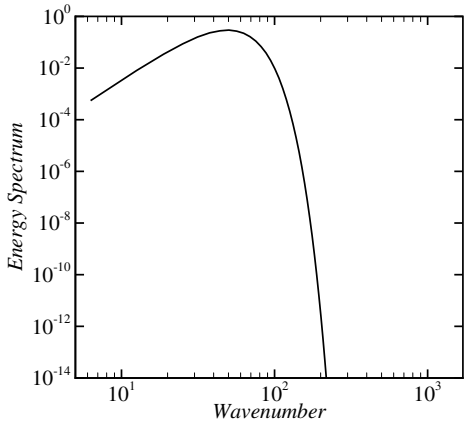

Fig. 5. Plot of the energy spectrum for the initial condition of the DNS of turbulence.

Fig. 6 describes the comparison of the energy spectrum between the IDO-SC scheme and the spectral method at an eddy turnover time ETT = 1.5. The energy spectrum obtained by the IDO-SC scheme shows quite good agreement with that of the spectral method for all the wavenumbers. Fig. 7(a)–(c) show the turbulence statistical

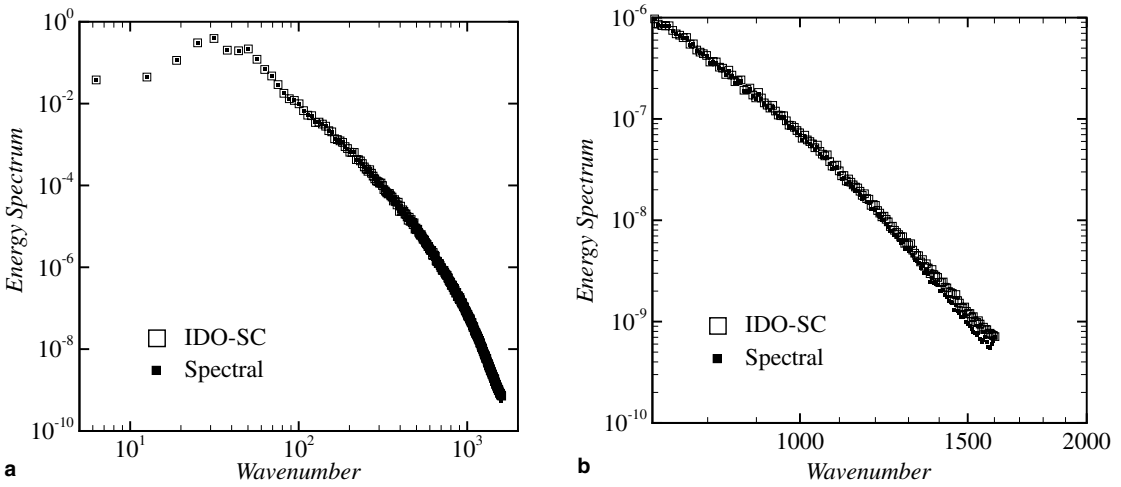

Fig. 6. Energy spectrum comparison between the IDO-SC scheme and the spectral method for ETT = 1.5: (a) all wavenumber region; (b) high wavenumber region.

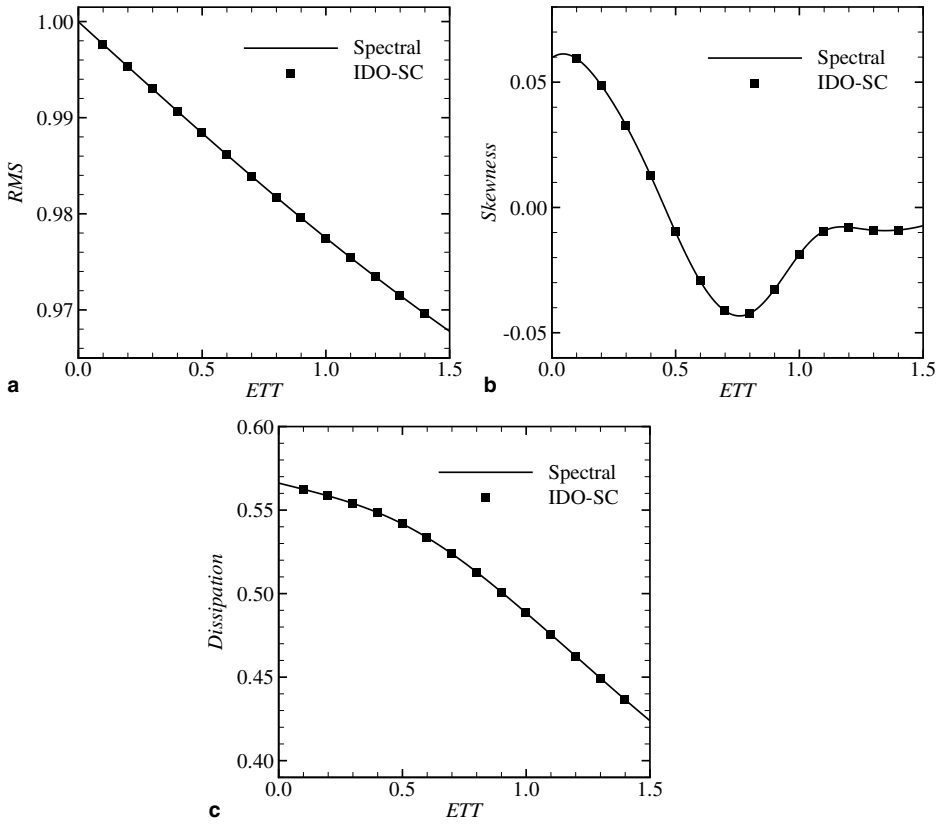

Fig. 7. Time histories of turbulence statistics: (a) root mean square of the velocity; (b) skewness of the x-directional velocity; (c) dissipation.

quantities of the root mean square of the velocity, the skewness of the horizontal velocity, and the dissipation, respectively. These results of the IDO-SC scheme completely follow the solid lines representing those of the spectral method. For the other statistical quantities, such as the flatness of the velocity, Kolmogorov scale, Taylor micro-scale etc., the IDO-SC scheme agrees with the spectral method. These agreements clearly show that the IDO-SC scheme retains a resolution comparable to that of spectral methods for incompressible flow simulations.

5.2. Two-dimensional driven cavity flow

Two-dimensional driven cavity flow is often studied as a benchmark test in incompressible flow simulation with use of Eqs. (5.1) and (5.2). To decrease CPU time in the cavity flow simulation, the following procedure is applied. First, we solve the advection and diffusion terms of Eq. (5.1) by using a four-stage Runge–Kutta method:

$$\mathbf{u}^* = \mathbf{u}^n + \sum_p^4 \beta_p \mathbf{k}_p \Delta t, \tag{5.8}$$

$$\mathbf{k}_p = -(\mathbf{u}^p \cdot \nabla)\mathbf{u}^p + \frac{1}{Re}\nabla^2 \mathbf{u}^p. \tag{5.9}$$

The advection term of Eq. (5.9) is discretized with the third-order upwind interpolation function. Then, the flow velocity at the next time step is corrected with the following equations:

$$\mathbf{u}^{n+1} = \mathbf{u}^* - \nabla p \Delta t, \tag{5.10}$$

$$\nabla \cdot \mathbf{u}^{n+1} = \nabla \cdot \mathbf{u}^* - \nabla^2 p \Delta t = 0. \tag{5.11}$$

Fig. 8(a) shows the results of the conventional IDO scheme on 40×40 uniform collocated grids with Reynolds number $\mathrm{Re} = 3200$ for the horizontal velocity u along the vertical axis with $x = 0.5$, which is the geometrical center in the horizontal direction, and the vertical velocity v along the horizontal axis with $y = 0.5$. As a reference, the velocity profiles of Ghia et al. [22] are shown. The conventional IDO scheme gives an inadequate result because of the poor coupling between velocity and pressure. The velocity profiles of the IDO-SC scheme on 40×40 collocated grids are in good agreement with the reference profile as shown in Fig. 8(b). We also plot the velocity profiles for $Re = 5000$ and $Re = 10{,}000$ in Fig. 9(a) and (b), respectively. It should be noted that uniform 56×56 grids for $Re = 5000$ and 80×80 grids for $Re = 10{,}000$ are used in these calculations. The IDO-SC scheme provides almost equal results with significantly smaller grid points in comparison with those of Ghia et al. on a 256×256 multigrid even for high Reynolds numbers.

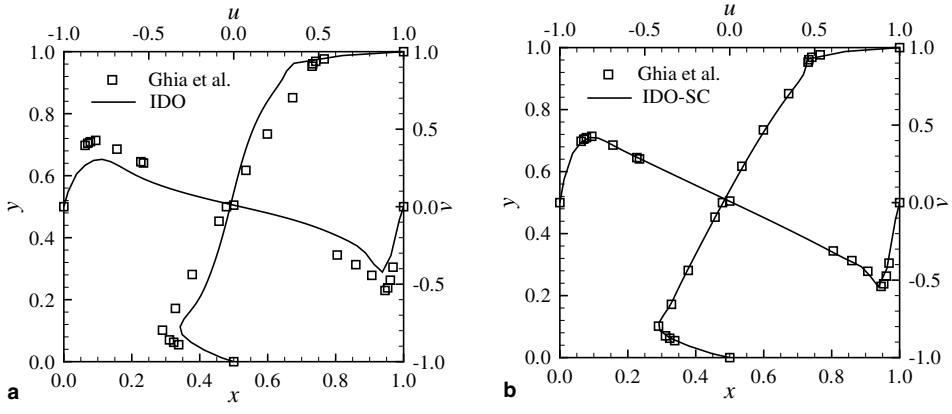

Fig. 8. Velocity profiles of cavity flow for Reynolds number 3200 with 40×40 collocated grids: (a) the conventional IDO scheme; (b) the IDO-SC scheme.

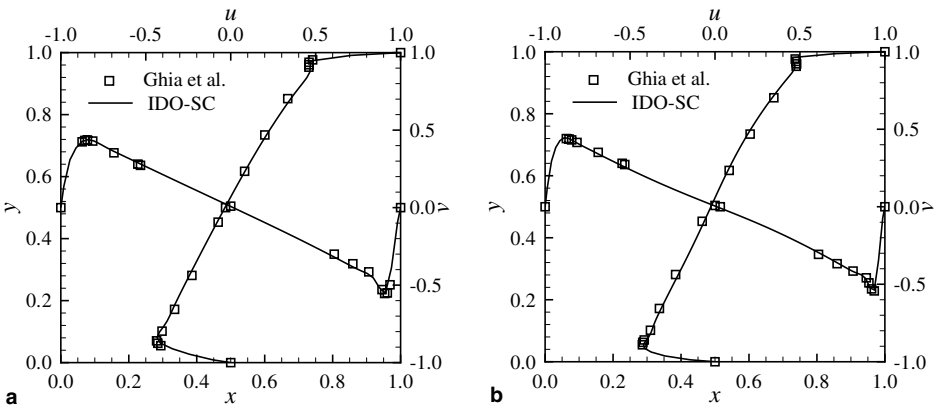

Fig. 9. Velocity profiles of cavity flows: (a) Reynolds number 5000 with 56×56 grids; (b) Reynolds number 10,000 with 80×80 grids.

6. Compressible flow problem

6.1. Formulation of the IDO-SC scheme for physical variables

In compressible flow problems, density and pressure change rapidly, and the coupling between the density (pressure) and the velocity becomes more important for stable calculations. The Euler equations for compressible flows are written as follows:

$$\frac{\partial \rho}{\partial t} = -u\frac{\partial \rho}{\partial x} - \rho\frac{\partial u}{\partial x}, \tag{6.1}$$

$$\frac{\partial u}{\partial t} = -u\frac{\partial u}{\partial x} - \frac{1}{\rho}\frac{\partial p}{\partial x}, \tag{6.2}$$

$$\frac{\partial e}{\partial t} = -u\frac{\partial e}{\partial x} - \frac{p}{\rho}\frac{\partial u}{\partial x}, \tag{6.3}$$

where the notation ρ denotes the density and e is the inertial energy. The same SC manner with the shallow water case is introduced in the last term of each equation. Eq. (6.2) is used for the time integration of the velocity, where the density is included in the last term. We need to improve the coupling between the velocity and the density. A discretized expression is thus derived for physical variables by using the third-order interpolation function,

$$F(X) = D_3X^3 + D_2X^2 + D_1X + D_0. \tag{6.4}$$

We determine the unknown coefficients by the four constraints of $F(\pm h) = f_{j\pm1}$ and $F_x(\pm h) = f_{x,j\pm1}$:

$$D_3 = -\frac{1}{4h^3}(f_{j+1} - f_{j-1}) + \frac{1}{4h^2}(f_{x,j+1} + f_{x,j-1}), \tag{6.5}$$

$$D_2 = \frac{1}{4h}(f_{x,j+1} - f_{x,j-1}), \tag{6.6}$$

$$D_1 = \frac{3}{4h}(f_{j+1} - f_{j-1}) - \frac{1}{4}(f_{x,j+1} + f_{x,j-1}), \tag{6.7}$$

$$D_0 = \frac{1}{2}(f_{j+1} + f_{j-1}) - \frac{h}{4}(f_{x,j+1} - f_{x,j-1}). \tag{6.8}$$

The physical variable and its first-order derivative at $x = x_j$ are given by $f(x_j) = F(0) = D_0$ and $f_x(x_j) = F_x(0) = D_1$. The weighted averages of these values and those of the fifth-order interpolation function (2.14) are

$$f(x_j) = (1-\gamma)B_0 + \gamma D_0 \tag{6.9}$$

and

$$f_x(x_j) = (1-\delta)B_1 + \delta D_1. \tag{6.10}$$

Since D_1 is the same as C_1, the above expression (6.10) coincides with SC representation (2.31) with the weighted parameter $\delta = 2/3$. By substituting $\gamma = 2/3$, the following representation is derived:

$$f(x_j) = \frac{1}{3}(f_{j+1} + f_j + f_{j-1}) - \frac{h}{6}(f_{x,j+1} - f_{x,j-1}). \tag{6.11}$$

The density profile is considered to be the combination of the fifth-order interpolation function (2.14) and the third-order interpolation function (6.4). The representation includes fourth-order truncation error:

$$f(x_j) = \frac{1}{3}(f_{j+1} + f_j + f_{j-1}) - \frac{h}{6}(f_{x,j+1} - f_{x,j-1}) + \frac{1}{36}\frac{\partial^4 f}{\partial x^4}h^4. \tag{6.12}$$

6.2. The IDO-SCR scheme

The IDO-SC scheme is not a monotone scheme, so that overshooting and undershooting appear at the edge of a discontinuity profile. Calculations of shock waves with the initial conditions of extreme density and pressure ratio sometimes break down due to a negative density. Xiao et al. [23] proposed the CIP scheme using a rational function (RCIP scheme) to prevent numerical oscillations for advection calculations. We adopt the rational function for the IDO-SC scheme, and call the scheme the IDO-SCR scheme. The following rational function is used:

$$F(X') = \frac{E_3 X'^3 + E_2 X'^2 + E_1 X' + E_0}{1 + RX'}, \tag{6.13}$$

$$R = \frac{|(S - f_{x,j-1})/(f_{x,j+1} - S)| - 1}{2h}, \tag{6.14}$$

$$S = \frac{f_{j+1} - f_{j-1}}{2h}, \tag{6.15}$$

where $X' = x - x_{j-1}$. The coefficients are determined by the same procedure as [23] for the constraints of $F(0) = f_{j-1}$, $F(2h) = f_{j+1}$, $F_x(0) = f_{x,j-1}$, and $F_x(2h) = f_{x,j+1}$.

$$E_3 = -\frac{1+Rh}{4h^3}(f_{j+1} - f_{j-1}) + \frac{1+2Rh}{4h^2}f_{x,j+1} + \frac{1}{4h^2}f_{x,j-1}, \tag{6.16}$$

$$E_2 = \frac{3+4Rh}{4h^2}(f_{j+1} - f_{j-1}) - \frac{1+2Rh}{2h}f_{x,j+1} - \frac{1}{h}f_{x,j-1}, \tag{6.17}$$

$$E_1 = Rf_{j-1} + f_{x,j-1}, \tag{6.18}$$

$$E_0 = f_{j-1}. \tag{6.19}$$

The physical variable and first-order derivative at the center $x = x_j$ of the interpolation domain are given as $f(x_j) = F(h)$, and $f_x(x_j) = F_x(h)$. When these variables are substituted into Eqs. (6.9) and (6.10) instead of D_0 and D_1, the discretized expressions of the IDO-SCR scheme are obtained:

$$f(x_j) = \frac{3-G}{6}f_{j+1} + \frac{1}{3}f_j + \frac{1+G}{6}f_{j-1} - \frac{(2-G)h}{6}f_{x,j+1} + \frac{Gh}{6}f_{x,j-1}, \tag{6.20}$$

$$f_x(x_j) = \frac{2+2G-G^2}{6h}(f_{j+1} - f_{j-1}) - \frac{2G-G^2}{6}(f_{x,j+1} + f_{x,j-1}) + \frac{1}{3}f_{x,j}, \tag{6.21}$$

$$G = \frac{1}{1+Rh}. \tag{6.22}$$

6.3. Shock tube problem

In order to confirm the effectiveness of the IDO-SCR scheme for compressible fluid flows, we examine one-dimensional shock tube problems. Since it is necessary to avoid undershooting of the density profile, we

choose the fractional steps method [24]. The governing equations (6.1)–(6.3) are divided into an advection phase and non-advection phase. First, the advection phase is time integrated by using the semi-Lagrangian procedure,

$$\rho_j^* = \rho(x_j - u_j\Delta t), \tag{6.23}$$

$$u_j^* = u(x_j - u_j\Delta t), \tag{6.24}$$

$$e_j^* = e(x_j - u_j\Delta t). \tag{6.25}$$

The RCIP scheme is used for ρ and e, and the CIP scheme is used for u because there is no need of monotonicity for u. Next, the equations for the non-advection phase,

$$\frac{\partial \rho}{\partial t} = -\rho_j^* u_{x,j}^{*\mathrm{SC}}, \tag{6.26}$$

$$\frac{\partial u}{\partial t} = -\frac{1}{\rho_j^{*\mathrm{SCR}}}(p_{x,j}^{*\mathrm{SCR}} + q_{x,j}^*), \tag{6.27}$$

$$\frac{\partial e}{\partial t} = -\frac{(p_j^* + q_j^*)}{\rho_j^*} u_{x,j}^{*\mathrm{SC}}, \tag{6.28}$$

are time advanced using a four-stage Runge–Kutta method. We apply the SC discretization to the values indicated by the superscript 'SC'. The values with the notation 'SCR' are replaced with the SCR discretization. In these equations, the variable q is added to the pressure as artificial viscosity [25], because we solve the compressible flow equations in a non-conservative form [26]. We also time integrate the equations for the first-order derivatives as done in the previous sections.

Fig. 10 shows the numerical results of density and pressure profiles with the initial condition of $\rho_L = 1.0$, $\rho_R = 0.125$, $p_L = 1.0$, $p_R = 0.1$, and $u_L = u_R = 0.0$. The uniform grid spacing is $h = 1/200$, the Courant number is 0.2, and the coefficient of artificial viscosity is 0.75. Collocated grids cannot be applied to this problem with the conventional IDO scheme, because the calculation breaks down just after the start. The IDO-SCR scheme solves the problem without numerical oscillations, and improves accuracy in comparison to the computation with staggered grids. It is found that our scheme gives comparable or better accuracy than other high-resolution schemes [27–29].

The results for very rare density and pressure on the right-hand side of the computational domain, that is, the density and pressure profiles initially have $\rho_L = 1.0$, $\rho_R = 1.0 \times 10^{-3}$, $p_L = 1.0$, $p_R = 1.0 \times 10^{-4}$, and $u_L = u_R = 0.0$, are illustrated in Fig. 11. The grid spacing is $h = 1/2000$, the Courant number is 0.2, and the coefficient of artificial viscosity is 2.0. It is noticed that the results of the IDO-SCR scheme are in good agreement with the exact solution for the situation of drastic density and pressure changes.

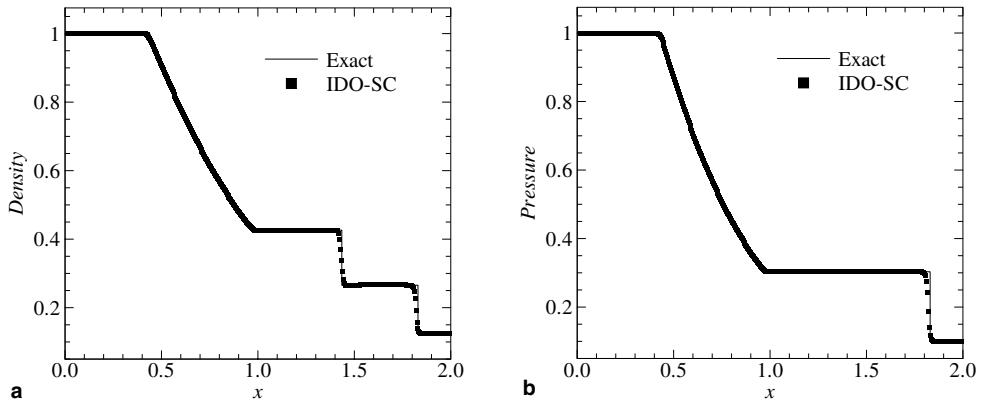

Fig. 10. Numerical results for the shock tube problem: (a) density; (b) pressure.

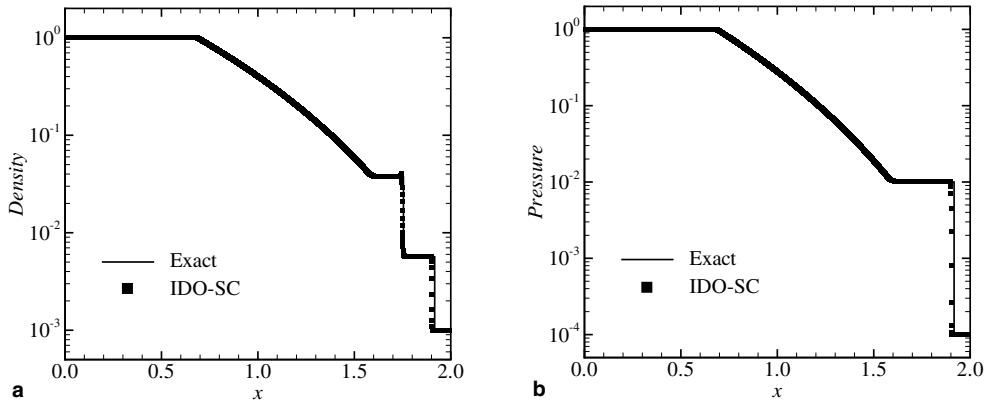

Fig. 11. Numerical results for strong shock: (a) density; (b) pressure.

7. Conclusions

We have presented a stable coupling method of the IDO scheme on collocated grids. A representation of first-order derivatives used in the IDO-SC scheme has fourth-order accuracy. Fourier analysis shows the IDO-SC scheme can resolve a wider range of wavenumbers than FD and CD schemes. In the shallow water problem of a hydrostatic meteorological model, the IDO-SC scheme drastically improves accuracy and stability in comparison with the conventional IDO scheme. DNS of two-dimensional homogeneous isotropic turbulence shows that the proposed scheme has a resolution comparable to that of spectral methods. For two-dimensional cavity flow problem, the results almost equal to those of Ghia et al. are achieved with significantly smaller grid numbers. We introduced a rational function into the SC method for solving compressible flow equations. The IDO-SCR scheme is applicable to calculations of strong shock waves with the initial condition of extremely large density and pressure jumps. The rational function not only suppresses numerical oscillations but also preserves the stability for such severe calculations. It is concluded that the proposed stable coupling method strongly contributes to improve the numerical stability and accuracy for fluid flow analysis of the IDO scheme on collocated grids.

Acknowledgement

We thank Dr. James Koga at the Japan Atomic Energy Research Institute for his helpful suggestions. This work was partly supported by Grant-in-Aid for Scientific Research (B) from the Japan Society for the Promotion of Science.

References

[1] T.E. Tezduyar, Stabilized finite element formulations for incompressible flow computations, Adv. Appl. Mech. 28 (1991) 1.
[2] T.E. Tezduyar, S. Mittal, S.E. Ray, R. Shih, Incompressible flow computations with stabilized bilinear and linear equal-order-interpolation velocity–pressure elements, Comput. Methods Appl. Mech. Engrg. 95 (1992) 221.
[3] F.H. Harlow, J.E. Welch, A numerical calculation of time dependent viscous incompressible flow of fluid with free surface, Phys. Fluids 8 (1965) 2182.
[4] S.V. Patankar, D.B. Spalding, A calculation procedure for heat, mass and momentum transfer in three-dimensional parabolic flows, Int. J. Heat Mass Transfer 15 (1972) 1787.
[5] T. Aoki, Interpolated Differential Operator (IDO) scheme for solving partial differential equations, Comput. Phys. Commun. 102 (1997) 132.
[6] T. Aoki, S. Nishita, K. Sakurai, Interpolated Differential Operator scheme and application to Level Set Method, Comput. Fluid Dynamics J. 9 (4) (2001) 418.
[7] T. Aoki, 3D simulation for falling papers, Comput. Phys. Commun. 142 (2001) 326.
[8] K. Sakurai, T. Aoki, W.H. Lee, K. Kato, Poisson equation solver with fourth-order accuracy by using Interpolated Differential Operator scheme, Comput. Math. Appl. 43 (2002) 621.
[9] S.K. Lele, Compact finite difference schemes with spectral-like resolution, J. Comput. Phys. 103 (1992) 16.

[10] M.J. Berger, J. Oliger, Adaptive mesh refinement for hyperbolic partial differential equations, J. Comput. Phys. 53 (1984) 484.
[11] M.J. Berger, P. Colella, Local adaptive mesh refinement for shock hydrodynamics, J. Comput. Phys. 82 (1989) 64.
[12] J.J. Quirk, An alternative to unstructured grids for computing gas dynamic flows around arbitrarily complex two-dimensional bodies, Comput. Fluids 23 (1994) 125.
[13] K. Sakurai, T. Aoki, A numerical procedure to evolving contact discontinuity by using moving Cut-Cell method, Comput. Fluid Dynamics J. 10 (1) (2001) 85.
[14] T. Yabe, T. Aoki, A universal solver for hyperbolic equations by cubic-polynomial interpolation: I. One-dimensional solver, Comput. Phys. Commun. 66 (1991) 219.
[15] T. Yabe, T. Ishikawa, P.Y. Wang, T. Aoki, Y. Kadota, F. Ikeda, A universal solver for hyperbolic equations by cubic-polynomial interpolation: II. Two- and three-dimensional solver, Comput. Phys. Commun. 66 (1991) 233.
[16] T. Yabe, F. Xiao, T. Utsumi, The constrained interpolation profile method for multiphase analysis, J. Comput. Phys. 169 (2001) 556.
[17] T. Aoki, Multi-dimensional advection of CIP (Cubic Interpolated Propagation) scheme, Comput. Fluid Dynamics J. 4 (3) (1995) 279.
[18] A. Staniforth, C. Temperton, Semi-implicit semi-Lagrangian integration schemes for a barotropic Finite-Element regional model, Mon. Wea. Rev. 114 (1985) 2078.
[19] C. Temperton, A. Staniforth, An efficient two-time-level semi-Lagrangian semi-implicit integration scheme, Quart. J. Roy. Meteor. Soc. 113 (1987) 1025.
[20] D. Gottlieb, A. Orszag, Numerical Analysis of Spectral Methods, SIAM, Philadelphia, 1977.
[21] A.A. Amsden, F.H. Harlow, A simplified MAC technique for incompressible fluid flow calculations, J. Comput. Phys. 6 (1970) 322.
[22] U. Ghia, K.N. Ghia, C.T. Shin, High-*Re* solution for incompressible flow using the Navier–Stokes equations and a multigrid method, J. Comput. Phys. 48 (1982) 387.
[23] F. Xiao, T. Yabe, T. Ito, Constructing oscillation preventing scheme for the advection equation by a rational function, Comput. Phys. Commun. 93 (1996) 1.
[24] J. Kim, P. Moin, Applications of a fractional steps method to incompressible Navier–Stokes equations, J. Comput. Phys. 59 (1985) 308.
[25] M.L. Wilkins, Use of artificial viscosity in multidimensional fluid dynamics calculations, J. Comput. Phys. 36 (1980) 281.
[26] K. Kato, T. Aoki, M. Yoshida, S. Kubota, A numerical scheme for strong blast wave driven by explosion, Int. J. Numer. Meth. Fluids, accepted.
[27] C.-W. Shu, S. Osher, S. Efficient, implementation of essentially non-oscillatory shock-capturing schemes, II, J. Comput. Phys. 83 (1989) 32.
[28] X.-D. Liu, S. Osher, T. Chan, Weighted essentially non-oscillatory schemes, J. Comput. Phys. 115 (1994) 200.
[29] G.-S. Jiang, C.-W. Shu, Efficient implementation of weighted ENO schemes, J. Comput. Phys. 126 (1996) 202.